



Cite this: *Phys. Chem. Chem. Phys.*,  
2015, 17, 10510

# Formation of 5- and 6-methyl-1*H*-indene (C<sub>10</sub>H<sub>10</sub>) via the reactions of the *para*-tolyl radical (C<sub>6</sub>H<sub>4</sub>CH<sub>3</sub>) with allene (H<sub>2</sub>CCCH<sub>2</sub>) and methylacetylene (HCCCH<sub>3</sub>) under single collision conditions

Tao Yang,<sup>a</sup> Dorian S. N. Parker,<sup>a</sup> Beni B. Dangi,<sup>a</sup> Ralf I. Kaiser\*<sup>a</sup> and  
Alexander M. Mebel\*<sup>b</sup>

The reactions of the *p*-tolyl radical with allene-d<sub>4</sub> and methylacetylene-d<sub>4</sub> as well as of the *p*-tolyl-d<sub>7</sub> radical with methylacetylene-d<sub>1</sub> and methylacetylene-d<sub>3</sub> were carried out under single collision conditions at collision energies of 44–48 kJ mol<sup>-1</sup> and combined with electronic structure and statistical (RRKM) calculations. Our experimental results indicated that the reactions of *p*-tolyl with allene-d<sub>4</sub> and methylacetylene-d<sub>4</sub> proceeded via indirect reaction dynamics with laboratory angular distributions spanning about 20° in the scattering plane. As a result, the center-of-mass translational energy distribution determined a reaction exoergicity of 149 ± 28 kJ mol<sup>-1</sup> and exhibited a pronounced maximum at around 20 to 30 kJ mol<sup>-1</sup>. In addition, the center-of-mass angular flux distribution *T*(θ) depicted a forward–backward symmetry and indicated geometric constraints upon the decomposing complex(es). Combining with calculations, these results propose that the bicyclic polycyclic aromatic hydrocarbons, 6-methyl-1*H*-indene (**p1**) and 5-methyl-1*H*-indene (**p2**), are formed under single collision conditions at fractions of at least 85% in both reaction systems. For the *p*-tolyl–methylacetylene system, experiments with partially deuterated reactants also reveal the formation of a third isomer **p5** (1-methyl-4-(1-propynyl)benzene) at levels of 5–10%, highlighting the importance in conducting reactions with partially deuterated reactants to elucidate the underlying reaction pathways comprehensively.

Received 23rd September 2014,  
Accepted 2nd March 2015

DOI: 10.1039/c4cp04288c

www.rsc.org/pccp

## 1. Introduction

Polycyclic aromatic hydrocarbons (PAHs) are ubiquitous in the interstellar medium (ISM).<sup>1–3</sup> They are regarded as the potential carriers of the diffuse interstellar bands (DIBs)<sup>4,5</sup> and the unidentified infrared emission bands (UIRs).<sup>5</sup> Currently PAHs and their derivatives such as cations, anions, and nitrogen-substituted PAHs (N-PAHs) are assumed to hold up to 10% of the interstellar carbon budget.<sup>6,7</sup> However, no individual PAH has been identified in the interstellar medium to date,<sup>8</sup> and hence the underlying formation mechanisms have still remained conjecture. In terrestrial environments, PAHs have been introduced into the environment via combustion of coals, biomass, and fossil fuels;<sup>9</sup> on Earth, PAHs are considered as toxic byproducts and have been characterized as carcinogenic,<sup>10–12</sup> mutagenic,<sup>12,13</sup> and teratogenic.<sup>12</sup> During recent years, the existence of PAHs in respiratory particulate matter (PM) has brought comprehensive impacts on

the urban areas, especially in developing countries such as China and Chile.<sup>14–16</sup> PAHs – also considered to be air and marine pollutants<sup>17–19</sup> – contribute to global warming as well.<sup>20</sup> Consequently, the increasing concerns about the impact of PAHs in terrestrial environments have propelled the combustion community to fully understand their formation mechanisms under combustion relevant conditions with the ultimate goal to eliminate these toxic byproducts from combustion systems.

Following stepwise molecular growth pathways, it is well established that resonantly stabilized free radicals (RSFRs)<sup>21–30</sup> as well as small aromatics like benzene (C<sub>6</sub>H<sub>6</sub>) and phenyl radicals (C<sub>6</sub>H<sub>5</sub>)<sup>30,31</sup> are crucial as precursors to PAH formation. Lindstedt *et al.* compiled competing formation mechanisms in the synthesis of the simplest bicyclic PAHs – indene (C<sub>9</sub>H<sub>8</sub>) and naphthalene (C<sub>10</sub>H<sub>8</sub>) – and incorporated these pathways into complex combustion models of fuel mixtures containing aromatic components.<sup>32</sup> Here, indene and naphthalene have been suggested to be formed via the hydrogen abstraction–acetylene addition (HACA) mechanism,<sup>31,33–36</sup> through the self-reaction of cyclopentadiene (C<sub>5</sub>H<sub>6</sub>)/cyclopentadienyl (C<sub>5</sub>H<sub>5</sub>),<sup>37–39</sup> or by the phenyl (benzene) addition–cyclization (PAC) mechanism with unsaturated hydrocarbons such as alkynes,<sup>40–44</sup> olefins

<sup>a</sup> Department of Chemistry, University of Hawaii at Manoa, Honolulu, Hawaii, USA.  
E-mail: ralfk@hawaii.edu; Tel: +1-808-956-5731

<sup>b</sup> Department of Chemistry and Biochemistry, Florida International University,  
Miami, Florida, USA. E-mail: mebel@fiu.edu; Tel: +1-305-348-1945

(olefinic radicals),<sup>35,43,45–47</sup> and aromatic molecules (aryl radicals).<sup>32,47–49</sup> Recently, our group initiated a systematic investigation on the reactions of the phenyl radicals with unsaturated hydrocarbons utilizing a photodissociation source and the crossed molecular beam approach.<sup>50–56</sup> We demonstrated that indene ( $C_9H_8$ ), naphthalene ( $C_{10}H_8$ ) as well as 1,4-dihydronaphthalene ( $C_{10}H_{10}$ ) can be formed respectively *via* the reactions of the phenyl radicals with allene ( $H_2CCCH_2$ ) and methylacetylene ( $CH_3CCH$ ),<sup>56</sup> vinylacetylene ( $H_2CCHCCH$ ),<sup>51</sup> and 1,3-butadiene ( $H_2CCHCHCH_2$ )<sup>53</sup> under single collision conditions (Fig. 1). These reactions were found to proceed through low entrance barriers (indene; 14 kJ mol<sup>-1</sup>) or were *de facto* barrierless to form initial van der Waals complexes, which then isomerized *via* submerged barriers (naphthalene, 1,4-dihydronaphthalene). Further, exploiting a chemical reactor at the Chemical Dynamics Beamline of the Advanced Light Source (ALS), Kaiser and Ahmed explored the reactions of phenyl radicals with methylacetylene ( $CH_3CCH$ )/allene ( $H_2CCCH_2$ ), acetylene ( $C_2H_2$ ), and 1,3-butadiene ( $C_4H_6$ ) and interrogated the reaction products *via* quasi continuous tunable vacuum ultraviolet (VUV) radiation and reflectron time-of-flight mass spectrometer (ReTOF). These studies identified reaction pathways to indene,<sup>57,58</sup> naphthalene,<sup>59</sup> and 1-methylindene ( $C_{10}H_{10}$ )<sup>58</sup> under combustion-like conditions at temperatures of typically 1000–1300 K and pressures of 300 Torr. The work also demonstrated experimentally

that naphthalene ( $C_{10}H_8$ ) can be formed *via* the hydrogen abstraction–acetylene addition (HACA) mechanism<sup>59</sup> providing a solid foundation to the understanding of PAH formation in combustion systems.

In crude oil, alkyl-substituted PAHs such as methyl-substituted naphthalenes and phenanthrenes are more abundant than non-substituted PAHs.<sup>60–64</sup> A recent crossed beam study on the reaction of *para*-tolyl ( $C_6H_4CH_3$ , *p*-tolyl) with vinylacetylene revealed the formation of 2-methylnaphthalene ( $C_{11}H_{10}$ )<sup>65</sup> indicating that the *p*-tolyl radical might act as a precursor in the reactions with unsaturated hydrocarbons toward the formation of alkyl-substituted PAHs (Fig. 1), including methyl substituted PAHs. Here, we are expanding these studies and explore potential formation pathways leading to methyl-substituted indene(s) *via* the reactions of *p*-tolyl with allene and methylacetylene under single collision conditions and combine these findings with electronic structure calculations. This work builds on our previous experience in forming indene under single collision conditions *via* the reactions of phenyl radicals with methylacetylene and allene by replacing a hydrogen atom in the phenyl radical reactant by a methyl group.

## 2. Experiment

We carried out the reactions of the *p*-tolyl radical ( $C_6H_4CH_3$ ;  $X^2A_1$ ) with allene-d4 ( $CD_2CCD_2$ ;  $X^1A_1$ ) and methylacetylene-d4 ( $CD_3CCD$ ;  $X^1A_1$ ), as well as of the *p*-tolyl-d7 radical ( $C_6D_4CD_3$ ;  $X^2A_1$ ) with methylacetylene-d1 ( $CH_3CCD$ ;  $X^1A_1$ ) and methylacetylene-d3 ( $CD_3CCH$ ;  $X^1A_1$ ) exploiting a universal crossed molecular beam machine under single collision conditions.<sup>66–69</sup> Helium gas (99.9999%; Airgas Gaspro) at a pressure 1.8 atm was introduced into a stainless steel bubbler containing *para*-chlorotoluene ( $C_7H_7Cl$ , 98%) or *para*-chlorotoluene-d7 ( $C_7D_7Cl$ , 98%). The seeded mixture was subsequently introduced into the primary source chamber *via* a pulsed piezo valve (Piezo Disk Translator; part number P-286.23; Physik Instrumente) operating at 120 Hz and driven by –400 V power supply. About 1 mm downstream from the pulsed valve nozzle, *p*-chlorotoluene was photolyzed by a 193 nm laser beam generated by a Lambda Physik Compex 110 Excimer laser operated at 60 Hz repetition rate with a pulse energy of  $18 \pm 2$  mJ focused to a 4 mm by 1 mm spot

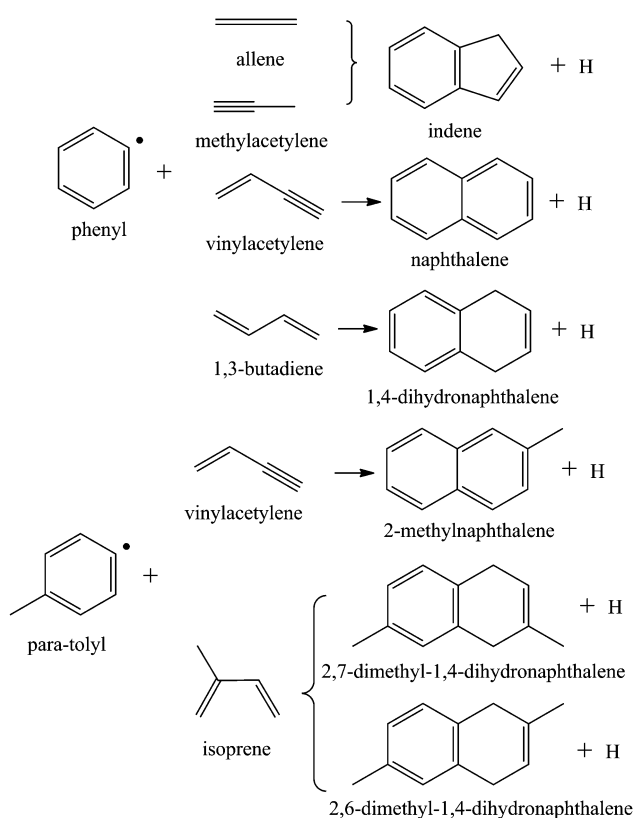


**Fig. 1** Formation of polycyclic aromatic hydrocarbons (PAHs) *via* reactions of phenyl-type radicals (phenyl/*para*-tolyl) with unsaturated hydrocarbons (allene, methylacetylene, vinylacetylene, 1,3-butadiene) using the crossed molecular beam method.

**Table 1** Primary and secondary beam peak velocities ( $v_p$ ), speed ratios ( $S$ ), collision energies ( $E_c$ ) and center-of-mass angles ( $\theta_{CM}$ ) for the reactions of the *p*-tolyl with methylacetylene-d4, *p*-tolyl with allene-d4, *p*-tolyl-d7 with methylacetylene-d1, and *p*-tolyl-d7 with methylacetylene-d3

Beam	$v_p$ (m s <sup>-1</sup> )	$S$	$E_c$ (kJ mol <sup>-1</sup> )	$\theta_{CM}$
<i>p</i> -C <sub>7</sub> H <sub>7</sub> (X <sup>2</sup> A <sub>1</sub> )	1605 ± 15	10.0 ± 0.8		
Allene-d4 (X <sup>1</sup> A <sub>1</sub> )	769 ± 18	8.0 ± 0.6	48 ± 3	13.1 ± 0.5
Methylacetylene-d4 (X <sup>1</sup> A <sub>1</sub> )	739 ± 18	8.0 ± 0.6	47 ± 3	12.7 ± 0.5
<i>p</i> -C <sub>7</sub> D <sub>7</sub> (X <sup>2</sup> A <sub>1</sub> )	1581 ± 15	14.5 ± 0.9		
Methylacetylene-d1 (X <sup>1</sup> A <sub>1</sub> )	749 ± 18	8.0 ± 0.6	44 ± 3	11.2 ± 0.5
Methylacetylene-d3 (X <sup>1</sup> A <sub>1</sub> )	749 ± 18	8.0 ± 0.6	47 ± 3	11.7 ± 0.5

rectangular spot.<sup>68</sup> A four-slot chopper wheel located after the skimmer selected a section of the *p*-tolyl radical beam with a well-defined peak velocity ( $v_p$ ) and speed ratio ( $S$ ) (Table 1). This section of the *p*-tolyl radical beam crossed then a second molecular beam of the closed shell hydrocarbon reactant released from a secondary pulsed valve perpendicularly. At a backing pressure of 550 Torr with a repetition frequency of 120 Hz and  $-400$  V pulse amplitude, allene-d4 ( $D_2CCCD_2$ ) and methylacetylene-d4 ( $DCCCD_3$ ) (for the reactions with *p*-tolyl) as well as methylacetylene-d1 ( $DCCCH_3$ ) and methylacetylene-d3 ( $HCCCD_3$ ) (for the reactions with *p*-tolyl-d7) were generated. Considering that both molecular beams have distinct velocities, the crossing of these segments was controlled by a pulse generator. The primary pulsed valve was triggered at 1870  $\mu$ s and the secondary pulsed valve was triggered 40  $\mu$ s prior to the primary pulsed valve. The excimer laser pulse was fired with a delay time of 180  $\mu$ s with respect to the primary pulsed valve.

Evacuated by a triple differentially pumping scheme to a pressure of a few  $10^{-12}$  Torr, the reactively scattered products were detected by electron-impact ionization of the neutral reaction products and mass separation exploiting a quadrupole mass spectrometer (QMS). The ionizer operated at 2 mA emission current ionizes the neutral products with an electron energy of 80 eV; the ionized product of a desired mass-to-charge ( $m/z$ ) ratio passes through the Extrel QC 150 quadrupole mass spectrometer. The ions are then accelerated towards a stainless steel 'door knob' target coated with an aluminum layer operated at  $-22.5$  kV, and initiate a cascade of electrons that fly towards an aluminum-coated organic scintillator eventually initiating photon release. Detected by a photomultiplier tube (PMT, Burle, Model 8850) operating at  $-1.35$  kV, the signal was filtered by a discriminator (Advanced Research Instruments, Model F-100TD, discrimination level: 1.6 mV), and then fed into a Stanford Research System SR430 multichannel scalar. The angular-resolved TOF spectra at a specific  $m/z$  ratio were recorded, integrated, and normalized to obtain the laboratory (LAB) product angular distribution. We further employed a forward-convolution routine and a set of initially parameterized functions of the product translational energy distribution  $P(E_T)$  and angular distribution  $T(\theta)$  in the center-of-mass (CM) frame, to iteratively fit the TOF spectra and the LAB angular distribution until the best fits are achieved.<sup>43,70,71</sup> In addition, we obtained the product flux contour map,  $I(\theta, u) = P(u) \times T(\theta)$ , which portrays the flux of the reactive scattering products ( $I$ ) as a function of the center-of-mass scattering angle ( $\theta$ ) and the product velocity ( $u$ ) in the CM frame. This plot represents the differential cross section and yields an 'image' of the reaction.<sup>72</sup>

## 3. Results

### 3.1. Laboratory data

Originally, we aimed to study the reactions of *p*-tolyl ( $C_7H_7$ ; 91 amu) with allene ( $H_2CCCH_2$ ; 40 amu) and methylacetylene ( $HCCCH_3$ ; 40 amu) to investigate the formation of distinct  $C_{10}H_{10}$  (130 amu) isomers. Unfortunately, significant non-reactive scattering signal was observed at  $m/z = 130$ , which originated from

the primary beam  $^{13}C_2C_5^{37}ClH_7$  ( $m/z = 130$ ) due to the natural abundance of  $^{13}C$  and  $^{37}Cl$ . To overcome this problem, we carried out the experiments *via* the reactions of *p*-tolyl ( $C_7H_7$ ; 91 amu) with allene-d4 ( $D_2CCCD_2$ ; 44 amu) and methylacetylene-d4 ( $DCCCD_3$ ; 44 amu), respectively. We collected TOF spectra of the product(s) at  $m/z = 134$  ( $C_{10}H_6D_4^+$ ), which corresponds to the atomic hydrogen loss channel, and  $m/z = 133$  ( $C_{10}H_7D_3^+/C_{10}H_5D_4^+$ ) accounting for the atomic deuterium loss channel as well as the dissociative ionization of potential product(s) from  $m/z = 134$  to  $m/z = 133$ . For the reaction of the *p*-tolyl radical with allene-d4 and methylacetylene-d4, we compared the reactive scattering signal at the center-of-mass angles and found that the signal intensity at  $m/z = 134$  originates principally from  $^{13}CC_9H_7D_3$ . The search for adducts with the molecular formula  $C_{10}H_7D_4$  ( $m/z = 135$ ) was also conducted, but no signal was found. Based on these findings, we collected angular-resolved TOF spectra at  $m/z = 133$  (Fig. 2). The TOF spectra were integrated and scaled according to the number of scans in order to derive the laboratory angular (LAB) distributions (Fig. 3). Based on these considerations, we can conclude that for the reaction of *p*-tolyl with allene-d4 and methylacetylene-d4, the atomic deuterium loss channel is open to forming product(s) with the molecular formula of  $C_{10}H_7D_3$ . Note that for both the reactions of *p*-tolyl with allene-d4 and methylacetylene-d4, the LAB angular distributions are very narrow and span only about  $20^\circ$  in the scattering plane defined by the primary and secondary beams.

It is important to outline that in the reaction of *p*-tolyl with methylacetylene-d4, the atomic deuterium emission can occur from either the acetylenic group or from the methyl group of methylacetylene. To ascertain the exact location of the atomic deuterium emission, the reactions of *p*-tolyl-d7 with partially-deuterated methylacetylenes should be investigated. Thus, we carried out the experiments on the atomic hydrogen and deuterium loss channels of *p*-tolyl-d7 reacting with methylacetylene-d1 ( $DCCCH_3$ ) and *p*-tolyl-d7 with methylacetylene-d3 ( $HCCCD_3$ ). We collected data at  $m/z = 138$  ( $C_{10}H_2D_8^+$ ) and 137 ( $C_{10}H_3D_7^+/C_{10}HD_8^+$ ) for the reaction of *p*-tolyl-d7 with methylacetylene-d1 at the CM angle of  $11.2^\circ$ . However, the signal at  $m/z$  of 137 had a strong background due to the precursor  $^{13}C_2C_5D_7^{37}Cl$  ( $m/z = 137$ ), and therefore we cannot obtain useful information on the deuterium loss channel from methylacetylene-d1. We also collected data at  $m/z = 140$  ( $C_{10}D_{10}^+$ ) and 139 ( $C_{10}HD_9^+$ ) for the reaction of *p*-tolyl-d7 with methylacetylene-d3 at the CM of  $11.7^\circ$ , which corresponds to the hydrogen and deuterium loss pathways, respectively. We found that the intensity of the signal at  $m/z = 139$  was about 1.3 times of that at  $m/z = 140$  (Fig. 4). In summary, we have shown that in the reactions of the *p*-tolyl-d7 radical with methylacetylene-d1 and methylacetylene-d3, the hydrogen atom may be lost both from the methyl group and from the acetylenic carbon atom of the methylacetylene molecule, with the hydrogen loss from methylacetylene-d1 enhanced by a factor of 1.4 compared to the signal from methylacetylene-d3.

### 3.2. Center-of-mass data

For both reactions of *p*-tolyl with methylacetylene-d4 and allene-d4, the laboratory data could be fit with the same the

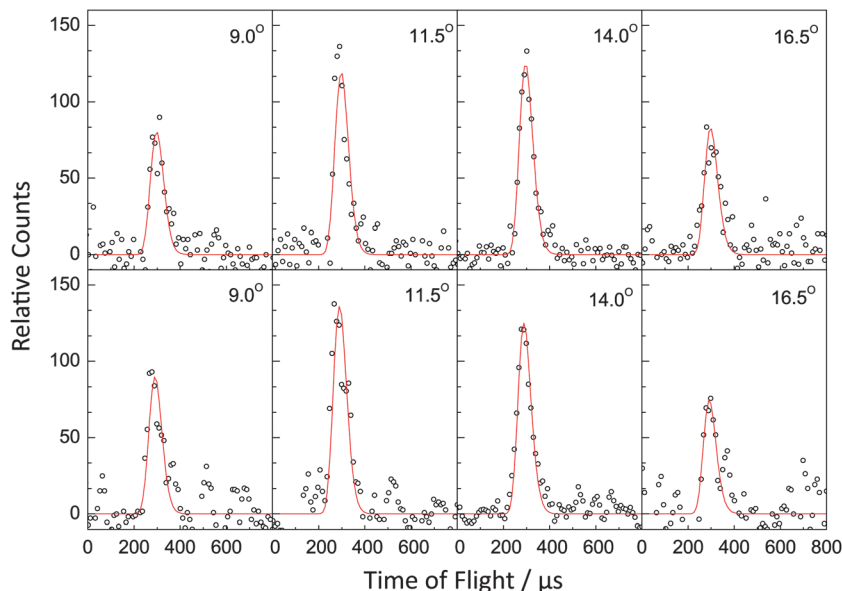


Fig. 2 Selected time-of-flight (TOF) spectra at mass-to-charge ( $m/z$ ) of 133 in the reactions of *p*-tolyl with allene- $d_4$  (top) and *p*-tolyl with methylacetylene- $d_4$  (bottom) via an atomic deuterium loss channel. The circles present the data points, while the solid lines represent the fits obtained from the forward-convolution routine.

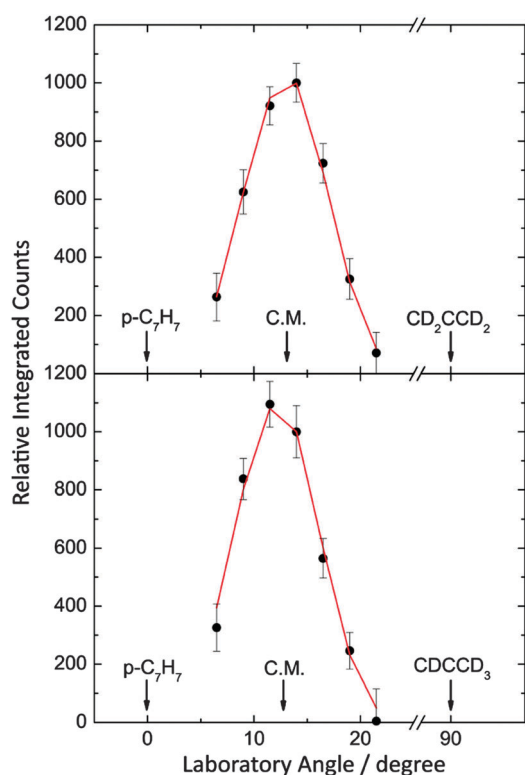


Fig. 3 Laboratory (LAB) angular distributions of ion signal at  $m/z = 133$  in the reactions of *p*-tolyl with allene- $d_4$  (top) and *p*-tolyl with methylacetylene- $d_4$  (bottom) via an atomic deuterium loss channel. The solid circles represent the experiment data, while the solid red lines represent the fits to the LAB angular distributions.

center-of-mass translational energy distribution reaching a maximum at  $196 \pm 24 \text{ kJ mol}^{-1}$  (Fig. 5). For those molecules born without internal excitation, this maximum translational

energy release represents the sum of the reaction energy and the collision energy. Since the collision energies of both systems are within  $47 \pm 4 \text{ kJ mol}^{-1}$ , we derive that the reactions leading to the formation of product(s) with the formula  $C_{10}H_7D_3$  are exoergic by  $149 \pm 28 \text{ kJ mol}^{-1}$ . Further, the available energy channelling into the translational degrees of freedom of the final products is  $82 \pm 11 \text{ kJ mol}^{-1}$  for both systems (about  $32 \pm 3\%$ ). In addition, the  $P(E_T)$  exhibits a pronounced maximum at around 20 to 30  $\text{kJ mol}^{-1}$ , which indicates that both systems possess tight exit barriers when the  $C_{10}H_7D_4$  intermediate(s) ejects a deuterium atom.

We can also obtain additional information on the center-of-mass angular flux distribution  $T(\theta)$  (Fig. 5). For both reaction systems,  $T(\theta)$  displays a distribution covering the full angular range from  $0^\circ$  to  $180^\circ$ , which indicates that the reactions follow indirect scattering dynamics involving the formation of  $C_{10}H_7D_4$  complex(es).<sup>73</sup> Also, the angular distribution is forward-backward symmetric with respect to  $90^\circ$ , implying that a decomposing complex has a lifetime that is longer than its rotational period.<sup>74</sup> The center-of-mass angular distribution is also peaked near  $90^\circ$  indicating the decomposing complex possesses geometric constraints upon the emission of a deuterium atom. Here, the decomposing intermediate(s)  $C_{10}H_7D_3$  ejects an atomic deuterium almost perpendicular to the rotational plane of the decomposing complex and nearly parallel to the total angular momentum vector ('sideway scattering').<sup>53</sup>

## 4. Theoretical results

The energies of all intermediates, transition states, and products for the fully-hydrogenated reaction system ( $C_{10}H_{11}$ ) are obtained at the G3(MP2,CC)//B3LYP/6-311G\*\* level of theory<sup>75</sup> using the GAUSSIAN 09<sup>76</sup> and MOLPRO 2010<sup>77</sup> program packages. This

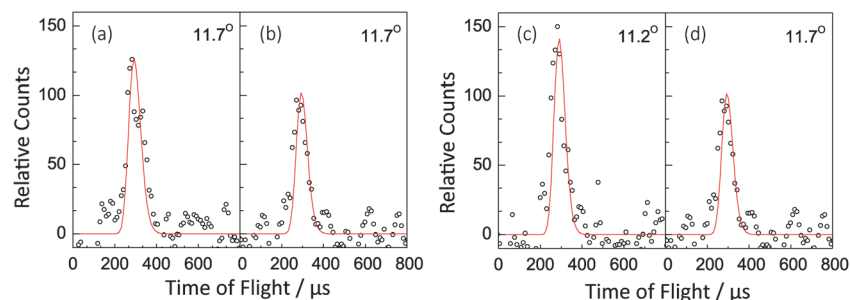


Fig. 4 The center-of-mass TOF data for the reaction of *p*-tolyl-d7 with methylacetylene-d3 at the  $m/z = 139$  ((a), D-loss) and 140 ((b), H-loss) and for the reaction of *p*-tolyl-d7 with methylacetylene-d1 and methylacetylene-d3 at  $m/z = 138$  ((c), H-loss) and  $m/z = 140$  ((d), H-loss), respectively.

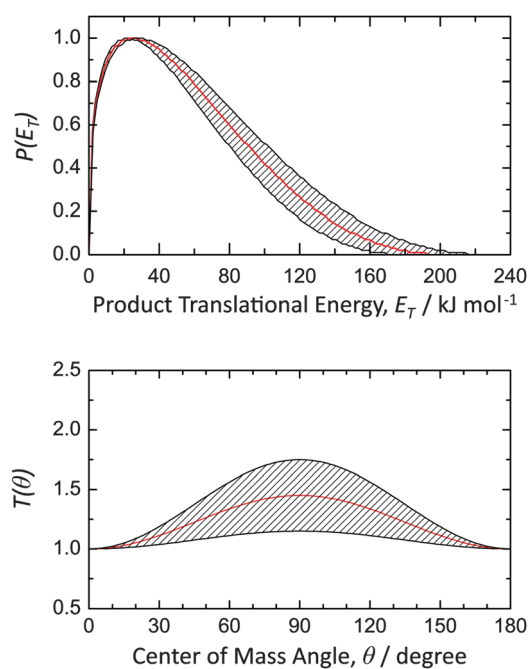


Fig. 5 Center-of-mass translational energy distribution  $P(E_T)$  (top) and angular distribution  $T(\theta)$  (bottom) for the formation of the  $C_{10}H_7D_3$  plus atomic deuterium product(s) via the reactions of the *p*-tolyl radical with allene-d4 and methylacetylene-d4. The hatched areas show the experimental error limits.

theoretical approach is expected to generate relative energies of various species within the accuracy of  $\pm 10 \text{ kJ mol}^{-1}$ .<sup>67</sup> Note that in our experiments the (partially) deuterated reactants are used, which can alter the zero point energies (ZPEs) by up to  $5 \text{ kJ mol}^{-1}$ , well within the errors of the calculations. Relative statistical yields (branching ratios) of various products were computed using energy-dependent rate constants of individual unimolecular reaction steps obtained from Rice–Ramsperger–Kassel–Marcus (RRKM) theory calculations utilizing the energetics and molecular parameters of reaction intermediates and transition states generated by the G3(MP2,CC)//B3LYP/6-311G\*\* calculations. The computational procedures are described in more detail elsewhere.<sup>70</sup>

The potential energy surface (PES) for the reaction of *p*-tolyl with allene and methylacetylene is illustrated in Fig. 6.

The calculations have identified 15 intermediates (**i1–i15**) and five reaction products (**p1–p5**). In the reaction of *p*-tolyl with methylacetylene, the *p*-tolyl radical attacks with its radical center at the sterically less-hindered C1 or at the C2 carbon atom of methylacetylene leading to the formation of intermediates **i1** and **i2**, respectively, via low entrance barrier of only  $11 \text{ kJ mol}^{-1}$  and  $17 \text{ kJ mol}^{-1}$ , respectively. Similarly, the initial addition of *p*-tolyl to the  $\pi$  electron density of allene results in two initial intermediates **i3** and **i4** through addition of the radical center to the C1 and C2 carbon atoms of allene via entrance barriers of  $10 \text{ kJ mol}^{-1}$  and  $15 \text{ kJ mol}^{-1}$ , respectively. For the reaction of *p*-tolyl and methylacetylene, **i1** can isomerize to intermediate **i5**, which can be regarded as the *trans*-form of **i1**. Considering the inherent barriers to isomerization of  $15 \text{ kJ mol}^{-1}$  and  $198 \text{ kJ mol}^{-1}$ , the 1,2-H shift in **i1** to **i12** does not compete with the rapid *cis–trans* isomerization **i1–i2**. The intermediate **i5** can then ring-close to a bicyclic intermediate **i6** via a barrier of  $123 \text{ kJ mol}^{-1}$  or isomerize to **i13** through a hydrogen migration from the methyl group of the methylacetylene moiety via a substantial barrier of  $179 \text{ kJ mol}^{-1}$ ; finally, **i5** can decompose to the product **p4** (1-methyl-4-propa-1,2-dienyl-benzene) plus an atomic hydrogen (with exoergicity of  $30 \text{ kJ mol}^{-1}$ ) or **p5** (1-methyl-4-(1-propynyl)benzene) plus an atomic hydrogen (with exoergicity of  $41 \text{ kJ mol}^{-1}$ ). Intermediate **i7** is generated by a ring opening in **i6** via a relatively low barrier of  $10 \text{ kJ mol}^{-1}$ ; essentially, the **i5–i7** isomerization occurs by migration of the *p*-tolyl moiety from C1 to C2 of methylacetylene. **i7** can follow two reaction pathways leading to intermediate **i4** via **i2** (*cis–trans* isomerization of the side chain followed by the 1,3-H shift from  $\text{CH}_3$  to  $\text{CH}$  in the side chain) and via **i11** (H migration from the aromatic ring to the  $\text{CH}$  group of the side chain followed by H migration from the methyl group in the side chain back to the ring); **i11** can also be formed by the addition of *p*-tolyl to allene at its C2 carbon atom. Intermediate **i4** consequently rearranges to **i8** by overcoming a barrier of  $157 \text{ kJ mol}^{-1}$  via a three-member ring closure and then **i8** ring-opens via a moderate barrier of  $37 \text{ kJ mol}^{-1}$  to form **i3**, which can be accessed via the addition of the *p*-tolyl radical center to the C1 carbon atom of the allene molecule. The **i4–i3** isomerization corresponds to migration of *p*-tolyl from C2 to C1 of allene. Essentially, both intermediates **i3** and **i4** can be accessed in one addition step from the *p*-tolyl–allene reactants or via multiple isomerizations from the *p*-tolyl–methylacetylene reactants.

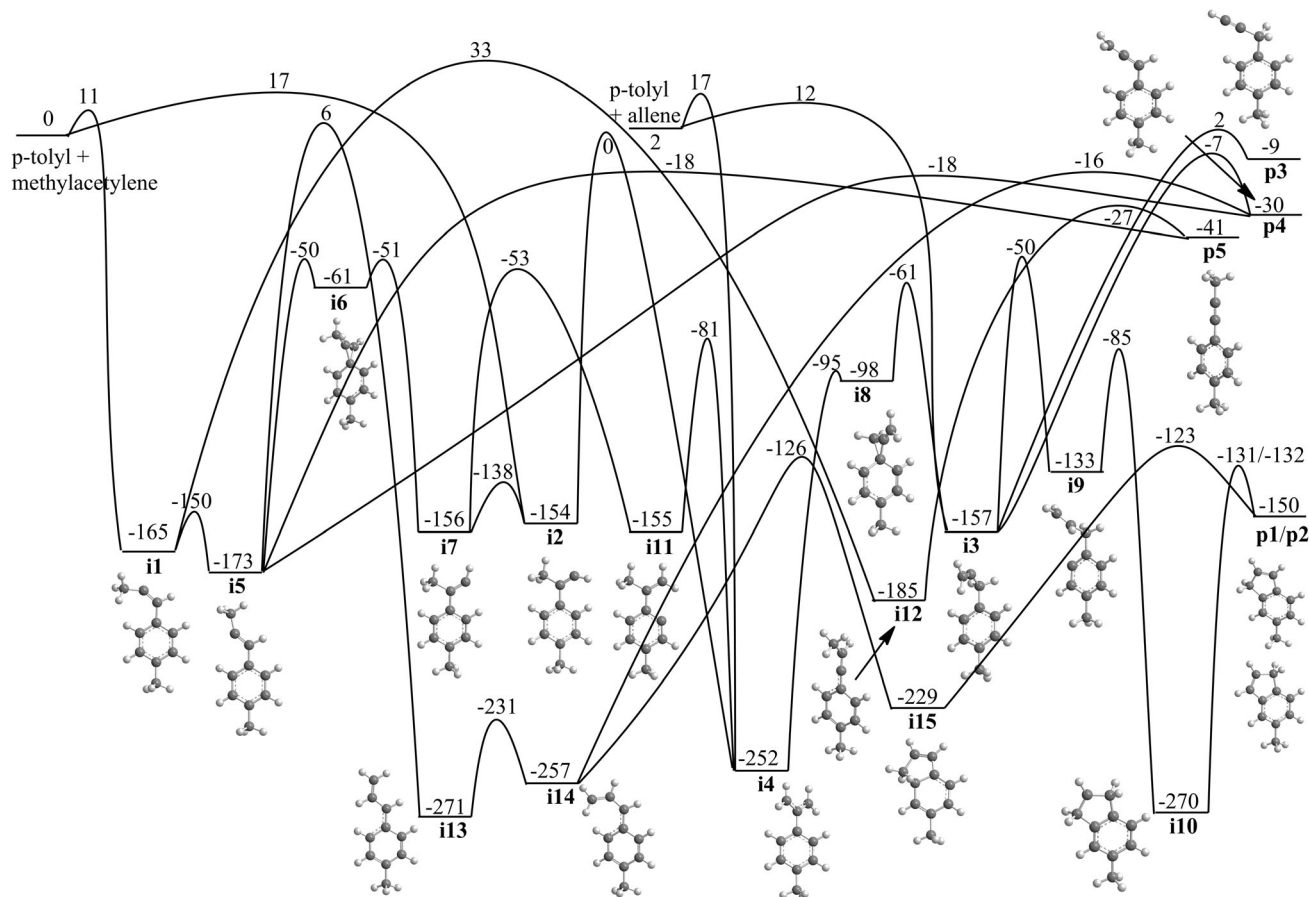


Fig. 6 Potential energy surface (PES) for the reaction of *p*-tolyl with methylacetylene and allene calculated at the G3(MP2,CC)//B3LYP/6-311G\*\* level of theory. All energies are given in kJ mol<sup>-1</sup>.

Intermediate **i3** can either decompose to the products **p3** (1-methyl-4-(2-propyn-1-yl)benzene) plus an atomic hydrogen (with exoergicity of 9 kJ mol<sup>-1</sup>) and **p4** plus an atomic hydrogen or undergo a hydrogen atom transfer from the *ortho* carbon atom of the *p*-tolyl radical (relative to the added side chain) to the C2 carbon atom of the allene moiety to form the intermediate **i9**. The latter undergoes five-member ring closure to yield intermediate **i10**. Eventually, **i10** can lose a hydrogen atom from either CH<sub>2</sub> group of the former allene moiety to yield two C<sub>10</sub>H<sub>10</sub> isomers: **p1** (6-methyl-1*H*-indene) and **p2** (5-methyl-1*H*-indene). Intermediate **i13**, another successor from **i5**, can be formed by 1,2-H migration from the CH<sub>3</sub> group in the methylacetylene moiety. Then **i3** follows the *cis*-*trans* isomerization to **i14** and the latter can either decompose to **p4** plus an atomic hydrogen, or undergo a five-member ring closure to form a bicyclic intermediate **i15**. Finally, **i15** can emit an atomic hydrogen from the CH group shared by the six-member and newly formed five-member rings to yield the product **p1**.

## 5. Discussion

Now we combine our experimental findings with the calculations to unveil the underlying reaction mechanism. First, the

experimentally-determined reaction exoergicity of  $149 \pm 28$  kJ mol<sup>-1</sup> matches very well with the computationally predicted reaction energy of  $150 \pm 5$  kJ mol<sup>-1</sup> to form 6-methyl-1*H*-indene (**p1**) and/or 5-methyl-1*H*-indene (**p2**). Therefore, we can conclude that at least the thermodynamically most stable methyl-1*H*-indene isomer(s) are formed in the reaction of the *p*-tolyl radical with methylacetylene and allene. Further, the order of magnitude of the experimentally predicted exit barrier of around 20 to 30 kJ mol<sup>-1</sup> correlates nicely with the computed exit barriers leading to **p1/p2** from **i10** (18 and 19 kJ mol<sup>-1</sup>) and/or **i15** (27 kJ mol<sup>-1</sup>). In addition, the geometric constraints of the deuterium loss (sideways scattering) also provide insights into the chemical reactions. Here, the computations depict that both in **ts**<sub>*i10*-*p1*</sub> and **ts**<sub>*i10*-*p2*</sub>, the deuterium atom is emitted at an angle of about 81.6° with respect to each molecular plane; for **ts**<sub>*i15*-*p1*</sub>, this emission takes place at an angle of about 94.7° (Fig. 7). Finally, we exploit RRKM calculations to predict the branching ratios (Table 2). At a collision energy of 47 kJ mol<sup>-1</sup>, RRKM calculations predict that the yield of **p1** and **p2** contributes up to 85.0%, 94.6%, 99.2% and 98.7% if the reaction starts from the initial collision complexes **i1**, **i2**, **i3**, and **i4**, respectively. Therefore, we can conclude that for the *p*-tolyl-allene system, 6-methyl-1*H*-indene (**p1**) and 5-methyl-1*H*-indene (**p2**) are the almost exclusive reaction products. On the other hand, for the

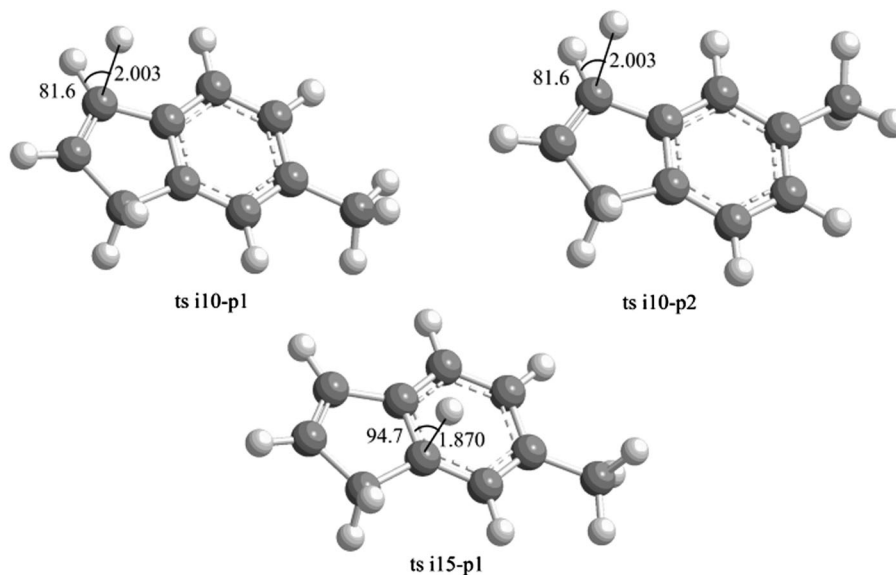


Fig. 7 Geometries of the exit transition states  $\text{ts}_{i10-p1}$ ,  $\text{ts}_{i10-p2}$  and  $\text{ts}_{i15-p1}$  leading to 6-methyl-1*H*-indene (**p1**) and 5-methyl-1*H*-indene (**p2**).

Table 2 Statistical branching ratios (%) of the products for the reactions of the *p*-tolyl radical with methylacetylene and allene at various collision energies. Here, **p1** to **p5** define 6-methyl-1*H*-indene, 5-methyl-1*H*-indene, 1-methyl-4-(2-propyn-1-yl)benzene, 1-methyl-4-propa-1,2-dienylbenzene, and 1-methyl-4-(1-propynyl)benzene

	Collision energy ( $\text{kJ mol}^{-1}$ )					
	12	22	32	42	47	52
From <b>i1</b>						
<b>p1</b> from <b>i10</b>	54.54	53.47	51.59	48.83	47.13	45.24
<b>p2</b> from <b>i10</b>	44.16	43.19	41.59	39.29	37.89	36.36
<b>p3</b>	0.00	0.00	0.01	0.02	0.03	0.05
<b>p4</b>	0.33	0.84	1.73	3.02	3.81	4.68
<b>p5</b>	0.98	2.49	5.08	8.84	11.14	13.65
<b>p1</b> from <b>i15</b>	$1.14 \times 10^{-3}$	$2.64 \times 10^{-3}$	$5.71 \times 10^{-3}$	$1.11 \times 10^{-2}$	$1.49 \times 10^{-2}$	$1.94 \times 10^{-2}$
From <b>i2</b>						
<b>p1</b> from <b>i10</b>	55.08	54.79	54.16	53.13	52.45	51.66
<b>p2</b> from <b>i10</b>	44.60	44.26	43.66	42.75	42.17	41.52
<b>p3</b>	0.00	0.00	0.01	0.02	0.03	0.05
<b>p4</b>	0.08	0.24	0.55	1.05	1.38	1.75
<b>p5</b>	0.24	0.71	1.61	3.04	3.96	5.01
<b>p1</b> from <b>i15</b>	$2.85 \times 10^{-4}$	$7.55 \times 10^{-4}$	$1.81 \times 10^{-3}$	$3.81 \times 10^{-3}$	$5.29 \times 10^{-3}$	$7.12 \times 10^{-3}$
From <b>i3</b>						
<b>p1</b> from <b>i10</b>	55.23	55.24	55.19	55.08	55.00	54.89
<b>p2</b> from <b>i10</b>	44.72	44.62	44.49	44.32	44.21	44.11
<b>p3</b>	0.00	0.00	0.01	0.02	0.04	0.06
<b>p4</b>	0.01	0.04	0.08	0.16	0.21	0.27
<b>p5</b>	0.04	0.10	0.22	0.41	0.53	0.67
<b>p1</b> from <b>i15</b>	$4.21 \times 10^{-5}$	$1.08 \times 10^{-4}$	$2.51 \times 10^{-4}$	$5.18 \times 10^{-4}$	$7.12 \times 10^{-4}$	$9.49 \times 10^{-4}$
From <b>i4</b>						
<b>p1</b> from <b>i10</b>	55.21	55.18	55.07	54.85	54.69	54.49
<b>p2</b> from <b>i10</b>	44.70	44.58	44.39	44.13	43.97	43.80
<b>p3</b>	0.00	0.00	0.01	0.02	0.03	0.06
<b>p4</b>	0.02	0.06	0.14	0.27	0.36	0.45
<b>p5</b>	0.06	0.18	0.39	0.73	0.95	1.19
<b>p1</b> from <b>i15</b>	$7.27 \times 10^{-5}$	$1.88 \times 10^{-4}$	$4.40 \times 10^{-4}$	$9.18 \times 10^{-4}$	$1.27 \times 10^{-4}$	$1.70 \times 10^{-4}$

reaction of *p*-tolyl with methylacetylene, only 85–95% of the products are 6-methyl-1*H*-indene (**p1**) and 5-methyl-1*H*-indene (**p2**). In order to test how sensitive the predicted branching fractions are to likely errors in the *ab initio* calculations we

carried out the following analysis. Since the computed relative energies of transition states are anticipated to be accurate within  $\pm 10 \text{ kJ mol}^{-1}$ , we considered the worst case scenario and increased the critical barrier heights on the pathways leading

to the formation of **p1/p2** (**i3** → **i9**, **i5** → **i6**, **i6** → **i7**, and **i7** → **i11**) by  $10 \text{ kJ mol}^{-1}$ , decreased the critical barriers leading to **p4** and **p5** (**i5** → **p4**, **i5** → **p5**, and **i3** → **p4**) by  $10 \text{ kJ mol}^{-1}$ , and recomputed rate constants and branching ratios. The results showed that for the reaction of *p*-tolyl with allene the branching ratios are nearly insensitive to such errors. The calculated relative yields of **p4** and **p5** slightly increase (to 2–3%), whereas the overall yield of **p1/p2** decreases to ~94%. The results for the reaction with methylacetylene appeared to be more sensitive to the possible errors in the barrier heights. If the reaction starts from **i2** the branching ratios of **p4** and **p5** increase to 8% and 21%, respectively, and the total **p1/p2** yield drops to 71%. Moreover, if the reaction starts from **i1**, the introduced corrections in the barrier heights make **p4** and **p5** the major reaction products (23% and 67%, respectively) and decrease the **p1/p2** to 10%. While the occurrence of the maximal errors in opposite directions is rather unlikely, this analysis illustrates that the yield of the **p4** and **p5** products in the *p*-tolyl + methylacetylene reaction can be significant. Recall that reactions with partially deuterated methylacetylene-d3 and methylacetylene-d1 depicted two distinct hydrogen losses. Considering the reaction sequence **i1** → **i5** → **p5** + H, the atomic hydrogen loss signal in the reaction of the *p*-tolyl radical with methylacetylene-d3 should form **p5** (1-methyl-4-(1-propynyl)benzene) (Fig. 6). Actually, we conducted a two-channel fitting on the two product systems: **p1/p2** ( $\text{C}_{10}\text{D}_{10}$ ) plus hydrogen (H) and **p5** ( $\text{C}_{10}\text{D}_{10}$ ) plus hydrogen (H), using two sets of CM parameterized functions with respect to each product system. We found that, the reaction channel leading to the formation of **p5** ( $\text{C}_{10}\text{D}_{10}$ ) plus an atomic hydrogen still accounts for up to 5–10% of the overall fit in the *p*-tolyl-d7 with methylacetylene-d3 system.

What are the underlying dynamics to form **p1/p2** ( $\text{C}_{10}\text{H}_7\text{D}_3$ ) under single collision conditions? Let us trace the deuterium atoms in the *p*-tolyl plus allene-d4 reaction. First, any addition of the *p*-tolyl radical will yield eventually **i3** – either from the reactants or *via* **i4** and **i8** involving *p*-tolyl migration. In **i3**, a hydrogen atom shifts from the *ortho* position of the tolyl ring to the C2 position of the allene moiety yielding **i9**. The latter undergoes ring closure to **i10**, in which the four deuterium atoms are pairwise found as  $\text{CD}_2$  groups. To regain closed shell structure, only a deuterium atom loss from **i10** can form 6-methyl-1*H*-indene (**p1**) and/or 5-methyl-1*H*-indene (**p2**). Therefore, both the computations and the experimental findings fully support the deuterium loss channel leading to the formation of 6-methyl-1*H*-indene (**p1**) and/or 5-methyl-1*H*-indene (**p2**) *via* the reaction sequence(s) (**i4** → **i8** →) **i3** → **i9** → **i10** → **p1/p2** + D. Note that the involvement of intermediate **i15** is unlikely. The reaction sequence **i13** → **i14** → **i15** → **p1/p2** + D links the *p*-tolyl-allene with the *p*-tolyl-methylacetylene surface *via* intermediate **i5**. However, the barrier involved in the **i5** → **i13** isomerization of  $179 \text{ kJ mol}^{-1}$  lies significantly higher than the competing isomerization from **i5** *via* **i6** to **i7**. Therefore, **i5** rather isomerizes *via* **i6** and **i7** eventually yielding **i11**, **i4**, and **i8** *via* energetically favorable transition states, which then eventually connect to **i3**. In the case of the *p*-tolyl-methylacetylene reaction, the situation is more complex and involves extensive

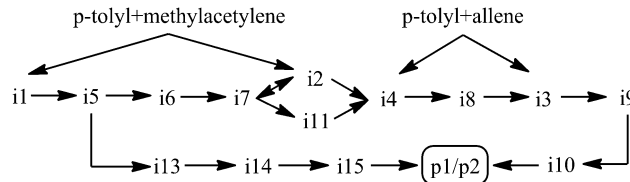


Fig. 8 Reaction schematic for the reactions of *p*-tolyl with methylacetylene and allene leading to the formation of products **p1** (6-methyl-1*H*-indene)/**p2** (5-methyl-1*H*-indene). The pathways involving **i13**, **i14**, and **i15** could be discounted for (see text for details).

isomerization pathways (Fig. 6 and 8). Here, the initial collision complexes **i1** and **i2** are essentially linked *via* the sequence **i1** → **i5** → **i6** → **i7** → **i2** → **i4** and **i1** → **i5** → **i6** → **i7** → **i11** → **i4** to intermediate **i4**, which is also accessible *via* addition of the *p*-tolyl radical to the central carbon atom of allene. In conclusion, the reactions of *p*-tolyl with allene and methylacetylene lead to the formation of 6-methyl-1*H*-indene (**p1**) and 5-methyl-1*H*-indene (**p2**) in yields of at least 85%. Intermediate **i3** can be classified as the pivotal reaction intermediate which eventually isomerizes *via* hydrogen shift and ring closure from **i9** to **i10** ultimately undergoing unimolecular decomposition to 6-methyl-1*H*-indene (**p1**) and 5-methyl-1*H*-indene (**p2**). Note that it is also enlightening to compare these systems with the reaction of the phenyl radicals with methylacetylene and allene.<sup>56</sup> Under the single collision conditions, these reactions involve also indirect scattering dynamics and lead predominantly to the formation of the indene molecule with yields of at least 85%. The replacement of a hydrogen atom in the phenyl radical by the methyl group in *para* position holds no significant consequences on the reaction dynamics, except the symmetry breaking from  $C_{2v}$  to  $C_s$  upon replacing a hydrogen atom by a methyl group in **i10**. This in turn results in the formation of two distinct methyl-substituted indene isomers 6-methyl-1*H*-indene (**p1**) and 5-methyl-1*H*-indene (**p2**).

## 6. Conclusion

We conducted the reactions of the *p*-tolyl radical with allene-d4 and methylacetylene-d4 as well as of the *p*-tolyl-d7 radical with methylacetylene-d1 and methylacetylene-d3 under single collision conditions at collision energies of  $44\text{--}48 \text{ kJ mol}^{-1}$ , and combined these studies with electronic structure and statistical (RRKM) calculations. Our experimental results indicated that the reactions of *p*-tolyl with allene-d4 and methylacetylene-d4 proceeded *via* indirect reaction dynamics with laboratory angular distributions spanning about  $20^\circ$  in the scattering plane, in an atomic deuterium loss pathway respectively. As a result, the experimentally-determined reaction exoergicity of  $149 \pm 28 \text{ kJ mol}^{-1}$  matches very well with the computationally predicted reaction energy of  $150 \pm 5 \text{ kJ mol}^{-1}$  to form 6-methyl-1*H*-indene (**p1**) and/or 5-methyl-1*H*-indene (**p2**). Also, the center-of-mass translational energy distribution exhibited a pronounced maximum at around  $20$  to  $30 \text{ kJ mol}^{-1}$ , implying that both systems possess tight exit barriers when the  $\text{C}_{10}\text{H}_7\text{D}_4$  intermediate(s) ejects a deuterium atom. In addition, the center-of-mass angular flux

distribution  $T(\theta)$  covered the full angular range from  $0^\circ$  to  $180^\circ$ , depicted a forward-backward symmetry and possessed geometric constraints upon the decomposing complex(es), which reflected the indirect reaction dynamics as well. Our calculations suggest that the bicyclic polycyclic aromatic hydrocarbons, 6-methyl-1*H*-indene and 5-methyl-1*H*-indene, are predominantly formed under single collision conditions at fractions of at least 85%. For the reactions of the *p*-tolyl radical with allene-d<sub>4</sub> and methylacetylene-d<sub>4</sub>, both reactions proceed *via* indirect scattering dynamics through complex formation by addition of the *p*-tolyl radical to the  $\pi$  electron density of the methylacetylene-d<sub>4</sub> and allene-d<sub>4</sub> reactants, respectively, yielding C<sub>10</sub>D<sub>4</sub>H<sub>7</sub> collision complexes. With respect to allene, both collision complexes could isomerize *via* a *de facto* *p*-tolyl group migration between the terminal and central carbon atoms followed by hydrogen migration from the *p*-tolyl moiety, ring closure, and deuterium loss forming 6-methyl-1*H*-indene (**p1**) and 5-methyl-1*H*-indene (**p2**) *via* tight exit transition states. Note that the collision complexes formed in the *p*-tolyl-methylacetylene system can be connected with those accessed *via* addition of the *p*-tolyl radical to the C1 and/or C2 allenic carbon atoms *via* successive isomerization (hydrogen shifts, *p*-tolyl group migration). In the *p*-tolyl-methylacetylene reaction, experiments with partially deuterated reactants also exposed the formation of a third isomer **p5** (1-methyl-4-(1-propynyl)benzene) at levels of 5–10% highlighting the importance in conducting reactions with partially deuterated reactants to elucidate the underlying reaction pathways comprehensively.

## Acknowledgements

This material is based upon work supported by the U.S. Department of Energy, Office of Basic Energy Sciences under Award Number DE-FG02-03ER15411 (Hawaii) and DE-FG02-04ER15570 (FIU). A.M.M. would like to acknowledge the Instructional & Research Computing Center (IRCC, web: <http://ircc.fiu.edu>) at Florida International University for providing HPC computing resources that have contributed to the research results reported within this paper.

## References

- 1 J. Postma, R. Hoekstra, A. Tielens and T. Schlathöler, *Astrophys. J.*, 2014, **783**, 61.
- 2 W. Duley, *Faraday Discuss.*, 2006, **133**, 415–425.
- 3 S. Lepp and A. Dalgarno, *Astrophys. J.*, 1988, **324**, 553–556.
- 4 G. H. Herbig, *Annu. Rev. Astron. Astrophys.*, 1995, **33**, 19–74.
- 5 A. Léger and L. d'Hendecourt, *Astron. Astrophys.*, 1985, **146**, 81–85.
- 6 A. G. Tielens, *Annu. Rev. Astron. Astrophys.*, 2008, **46**, 289–337.
- 7 P. Ehrenfreund and M. A. Sephton, *Faraday Discuss.*, 2006, **133**, 277–288.
- 8 C. Bauschlicher Jr, C. Boersma, A. Ricca, A. Mattioda, J. Cami, E. Peeters, F. S. de Armas, G. P. Saborido, D. Hudgins and L. Allamandola, *Astron. Astrophys., Suppl. Ser.*, 2010, **189**, 341.
- 9 S. Baek, R. Field, M. Goldstone, P. Kirk, J. Lester and R. Perry, *Water, Air, Soil Pollut.*, 1991, **60**, 279–300.
- 10 P. P. Fu, F. A. Beland and S. K. Yang, *Carcinogenesis*, 1980, **1**, 725–727.
- 11 W. F. Busby, E. K. Stevens, E. R. Kellenbach, J. Cornelisse and J. Lugtenburg, *Carcinogenesis*, 1988, **9**, 741–746.
- 12 K. H. Kim, S. A. Jahan, E. Kabir and R. J. C. Brown, *Environ. Int.*, 2013, **60**, 71–80.
- 13 J. L. Durant, W. F. Busby, A. L. Lafleur, B. W. Penman and C. L. Crespi, *Mutat. Res., Genet. Toxicol.*, 1996, **371**, 123–157.
- 14 M. Zheng, L. G. Salmon, J. J. Schauer, L. Zeng, C. Kiang, Y. Zhang and G. R. Cass, *Atmos. Environ.*, 2005, **39**, 3967–3976.
- 15 H. Guo, S. Lee, K. Ho, X. Wang and S. Zou, *Atmos. Environ.*, 2003, **37**, 5307–5317.
- 16 M. del Rosario Sienna, N. G. Rosazza and M. Préndez, *Atmos. Res.*, 2005, **75**, 267–281.
- 17 K. J. Hylland, *J. Toxicol. Environ. Health, Part A*, 2006, **69**, 109–123.
- 18 B. J. Finlayson-Pitts and J. N. Pitts Jr., *Science*, 1997, **276**, 1045–1052.
- 19 J. H. Seinfeld and J. F. Pankow, *Annu. Rev. Phys. Chem.*, 2003, **54**, 121–140.
- 20 R. J. Andres, T. A. Boden, F. M. Breon, P. Ciais, S. Davis, D. Erickson, J. S. Gregg, A. Jacobson, G. Marland and J. Miller, *et al.*, *Biogeosciences*, 2012, **9**, 1845–1871.
- 21 N. M. Marinov, W. J. Pitz, C. K. Westbrook, A. M. Vincitore, M. J. Castaldi, S. M. Senkan and C. F. Melius, *Combust. Flame*, 1998, **114**, 192–213.
- 22 R. Kaiser, D. Stranges, H. Bevsek, Y. Lee and A. Suits, *J. Chem. Phys.*, 1997, **106**, 4945–4953.
- 23 F. Stahl, P. Schleyer, H. Schaefer III and R. Kaiser, *Planet. Space Sci.*, 2002, **50**, 685–692.
- 24 R. I. Kaiser, N. Balucani, D. O. Charkin and A. M. Mebel, *Chem. Phys. Lett.*, 2003, **382**, 112–119.
- 25 N. Balucani, A. M. Mebel, Y. T. Lee and R. I. Kaiser, *J. Phys. Chem. A*, 2001, **105**, 9813–9818.
- 26 R. I. Kaiser, T. N. Le, T. L. Nguyen, A. M. Mebel, N. Balucani, Y. T. Lee, F. Stahl, P. v. R. Schleyer and H. F. Schaefer III, *Faraday Discuss.*, 2002, **119**, 51–66.
- 27 R. I. Kaiser, I. Hahndorf, L. C. L. Huang, Y. T. Lee, H. F. Bettinger, P. v. R. Schleyer, H. F. Schaefer III and P. R. Schreiner, *J. Chem. Phys.*, 1999, **110**, 6091–6094.
- 28 R. Kaiser, C. Chiong, O. Asvany, Y. Lee, F. Stahl, P. v. R. Schleyer and H. Schaefer III, *J. Chem. Phys.*, 2001, **114**, 3488–3496.
- 29 J. A. Miller, *Theory and modeling in combustion chemistry*, Symposium (International) on Combustion, Elsevier, 1996, pp. 461–480.
- 30 H. Richter and J. Howard, *Prog. Energy Combust. Sci.*, 2000, **26**, 565–608.
- 31 M. Frenklach, *Phys. Chem. Chem. Phys.*, 2002, **4**, 2028–2037.
- 32 P. Lindstedt, L. Maurice and M. Meyer, *Faraday Discuss.*, 2001, **119**, 409–432.

- 33 H. Wang and M. Frenklach, *J. Phys. Chem.*, 1994, **98**, 11465–11489.
- 34 V. V. Kislov, N. I. Islamova, A. M. Kolker, S. H. Lin and A. M. Mebel, *J. Chem. Theory Comput.*, 2005, **1**, 908–924.
- 35 L. Vereecken and J. Peeters, *Phys. Chem. Chem. Phys.*, 2003, **5**, 2807–2817.
- 36 G. d. Silva and J. W. Bozzelli, *J. Phys. Chem. A*, 2009, **113**, 8971–8978.
- 37 D. Wang, A. Violi, D. H. Kim and J. A. Mullholland, *J. Phys. Chem. A*, 2006, **110**, 4719–4725.
- 38 V. Kislov and A. Mebel, *J. Phys. Chem. A*, 2008, **112**, 700–716.
- 39 N. Marinov, W. Pitz, C. Westbrook, M. Castaldi and S. Senkan, *Combust. Sci. Technol.*, 1996, **116**, 211–287.
- 40 I. V. Tokmakov, J. Park and M. C. Lin, *ChemPhysChem*, 2005, **6**, 2075–2085.
- 41 L. Vereecken, J. Peeters, H. F. Bettinger, R. I. Kaiser, P. V. Schleyer and H. F. Schaefer, *J. Am. Chem. Soc.*, 2002, **124**, 2781–2789.
- 42 L. Vereecken, H. F. Bettinger and J. Peeters, *Phys. Chem. Chem. Phys.*, 2002, **4**, 2019–2027.
- 43 J. D. Bittner, PhD thesis, Massachusetts Institute of Technology, Cambridge, MA 02139, USA, 1981.
- 44 A. M. Mebel, V. V. Kislov and R. I. Kaiser, *J. Am. Chem. Soc.*, 2008, **130**, 13618–13629.
- 45 T. Yu and M. C. Lin, *Combust. Flame*, 1995, **100**, 169–176.
- 46 J. Park, G. J. Nam, I. V. Tokmakov and M. C. Lin, *J. Phys. Chem. A*, 2006, **110**, 8729–8735.
- 47 S. Fascella, C. Cavallotti, R. Rota and S. Carra, *J. Phys. Chem. A*, 2004, **108**, 3829–3843.
- 48 J. Park, S. Burova, A. S. Rodgers and M. C. Lin, *J. Phys. Chem. A*, 1999, **103**, 9036–9041.
- 49 M. Shukla, A. Susa, A. Miyoshi and M. Koshi, *J. Phys. Chem. A*, 2008, **112**, 2362–2369.
- 50 R. I. Kaiser, D. S. N. Parker, M. Goswami, F. Zhang, V. V. Kislov, A. M. Mebel, J. Aguilera-Iparraguirre and W. H. Green, *Phys. Chem. Chem. Phys.*, 2012, **14**, 720–729.
- 51 D. S. N. Parker, F. T. Zhang, Y. S. Kim, R. I. Kaiser, A. Landera, V. V. Kislov, A. M. Mebel and A. G. G. M. Tielens, *Proc. Natl. Acad. Sci. U. S. A.*, 2012, **109**, 53–58.
- 52 D. Parker, F. Zhang, Y. Kim, R. Kaiser, A. Landera and A. Mebel, *Phys. Chem. Chem. Phys.*, 2012, **14**, 2997–3003.
- 53 R. I. Kaiser, D. S. N. Parker, F. Zhang, A. Landera, V. V. Kislov and A. M. Mebel, *J. Phys. Chem. A*, 2012, **116**, 4248–4258.
- 54 D. S. Parker, T. Yang, R. I. Kaiser, A. Landera and A. M. Mebel, *Chem. Phys. Lett.*, 2014, **595**, 230–236.
- 55 T. Yang, D. S. N. Parker, B. B. Dangi, R. I. Kaiser, V. V. Kislov and A. M. Mebel, *J. Phys. Chem. A*, 2014, **118**, 4372–4381.
- 56 D. D. S. Parker, D. F. Zhang, D. R. I. Kaiser, D. V. V. Kislov and D. A. M. Mebel, *Chem. – Asian J.*, 2011, **6**, 3035.
- 57 F. Zhang, R. I. Kaiser, V. V. Kislov, A. M. Mebel, A. Golan and M. Ahmed, *J. Phys. Chem. Lett.*, 2011, **2**, 1731–1735.
- 58 A. Golan, M. Ahmed, A. M. Mebel and R. I. Kaiser, *Phys. Chem. Chem. Phys.*, 2013, **15**, 341–347.
- 59 D. S. Parker, R. I. Kaiser, T. P. Troy and M. Ahmed, *Angew. Chem., Int. Ed.*, 2014, **53**, 7740–7744.
- 60 Z. Wang, B. Hollebone, M. Fingas, L. Sigouin, B. Fieldhouse, M. Landriault, G. Thouin, J. Noonan and J. Weaver, *Int. Oil Spill Conf. Proc.*, 2003, **2003**, 1131–1138.
- 61 B. Yang, Y. Li, L. Wei, C. Huang, J. Wang, Z. Tian, R. Yang, L. Sheng, Y. Zhang and F. Qi, *Proc. Combust. Inst.*, 2007, **31**, 555–563.
- 62 C. Huang, L. Wei, B. Yang, J. Wang, Y. Li, L. Sheng, Y. Zhang and F. Qi, *Energy Fuels*, 2006, **20**, 1505–1513.
- 63 Y. Li, C. Huang, L. Wei, B. Yang, J. Wang, Z. Tian, T. Zhang, L. Sheng and F. Qi, *Energy Fuels*, 2007, **21**, 1931–1941.
- 64 Y. Y. Li, L. D. Zhang, Z. Y. Tian, T. Yuan, J. Wang, B. Yang and F. Qi, *Energy Fuels*, 2009, **23**, 1473–1485.
- 65 D. S. Parker, B. B. Dangi, R. I. Kaiser, A. Jamal, M. N. Ryazantsev, K. Morokuma, A. Korte and W. Sander, *J. Phys. Chem. A*, 2014, **118**, 2709–2718.
- 66 Y. Guo, X. B. Gu, E. Kawamura and R. I. Kaiser, *Rev. Sci. Instrum.*, 2006, **77**, 034701.
- 67 X. B. Gu, Y. Guo, F. T. Zhang, A. M. Mebel and R. I. Kaiser, *Faraday Discuss.*, 2006, **133**, 245–275.
- 68 R. I. Kaiser, P. Maksyutenko, C. Ennis, F. T. Zhang, X. B. Gu, S. P. Krishtal, A. M. Mebel, O. Kostko and M. Ahmed, *Faraday Discuss.*, 2010, **147**, 429–478.
- 69 F. T. Zhang, S. Kim and R. I. Kaiser, *Phys. Chem. Chem. Phys.*, 2009, **11**, 4707–4714.
- 70 P. S. Weiss, PhD thesis, University of California at Berkeley, Berkeley, California 94720, USA, 1986.
- 71 R. I. Kaiser, T. N. Le, T. L. Nguyen, A. M. Mebel, N. Balucani, Y. T. Lee, F. Stahl, P. V. Schleyer and H. F. Schaefer, *Faraday Discuss.*, 2001, **119**, 51–66.
- 72 R. L. Kaiser, D. S. N. Parker, F. Zhang, A. Landera, V. V. Kislov and A. M. Mebel, *J. Phys. Chem. A*, 2012, **116**, 4248–4258.
- 73 R. D. Levine, *Molecular Reaction Dynamics*, Cambridge University Press, Cambridge, UK, 2005.
- 74 W. B. Miller, S. A. Safron and D. R. Herschbach, *Discuss. Faraday Soc.*, 1967, **44**, 108–122.
- 75 L. A. Curtiss, K. Raghavachari, P. C. Redfern, A. G. Baboul and J. A. Pople, *Chem. Phys. Lett.*, 1999, **314**, 101–107.
- 76 M. Frisch, G. Trucks, H. B. Schlegel, G. Scuseria, M. Robb, J. Cheeseman, G. Scalmani, V. Barone, B. Mennucci and G. Petersson, *Gaussian 09, Revision A. 02*, Gaussian, 2009.
- 77 H. Werner, P. Knowles, R. Lindh, F. Manby, M. Schütz, P. Celani and T. Korona, *MOLPRO*, 2010.